ACTA ACUSTICA UNITED WITH ACUSTICA
Vol. 97 (2011) 1 – 1

The Influence of Geometrical and Mechanical Input Parameters on Theoretical Models of Phonation

J. Cisonni[1)], A. Van Hirtum[1)], X. Pelorson[1)], J. Lucero[2)]
[1)] GIPSA-lab, UMR CNRS 5216, Grenoble Universities, France. annemie.vanhirtum@gipsa-lab.grenoble-inp.fr
[2)] University of Brasilia, Brasil

Summary
The influence of initial aperture and mechanical properties on the onset pressure thresholds and oscillation frequencies is experimentally assessed on a deformable vocal fold replica in case of strong and weak acoustical coupling. The mechanical replica enables to vary the initial aperture while mechanical properties are maintained and therefore to mimic abduction and adduction gestures of human phonation. Depending on initial conditions (geometrical, mechanical and acoustical) one or two oscillation regions are experimentally found for which important differences are observed for both oscillation onset pressure thresholds and oscillation frequencies. Measured onset pressure thresholds are used to validate the outcome of a theoretical model of phonation using a reduced mechanical model. The applied coupling stiffness in the theoretical model is estimated from the measured frequency response instead of imposed by an 'ad-hoc' criterion. The variations in coupling stiffness result in a qualitative agreement between predicted and measured values for all assessed experimental conditions. In addition, the Young's modulus of the replica is qualitatively estimated to be within the range observed 'in-vivo'.

PACS no. 43.70.Bk, 43.70.Jt

Introduction

Theoretical phonation models aim to mimic the physiological fluid-structure interaction during vocal fold self-sustained oscillations. The relevance of phonation modeling requires a faithful triple relationship between 1) model parameters, 2) 'in-vivo' physiological meaningful variables and 3) 'in-vitro' measurable quantities. Simplified theoretical phonation models, like one or two mass models [1, 2, 3] are of interest for their limited number of input parameters favouring the relationship with 'in-vivo' physiological variables. Moreover, the incessant development of 'in-vivo' measurement techniques allows to quantify mechanical 'in-vivo' properties [4, 5].

In particular studying the models/system behaviour for varying parameters which can be controlled during 'in-vivo' speech utterances is of interest. Therefore, the subglottal pressure is varied since the subglottal pressure drives the pressure drop along the glottis and consequently the forces exerted by the flow on the surrounding walls at the origin of the fluid-structure interaction generating vocal folds self-sustained oscillations. Besides the driving pressure, variation of mechanical parameters and the initial aperture are important since they can be directly related to important physiological parameters such as muscle activity and are controlled 'in-vivo' at the voicing onset in speech utterances by laryngeal abduction and adduction gestures [6, 7, 8, 9].

Validation of theoretical models and their behavior in terms of accuracy, reproducibility and sensitivity to each individual parameter variation requires a suitable mechanical vocal fold replica and experimental setup. The use of an experimental setup allows focusing on the modeling of specific physical issues involved in the oscillatory cycle, which can hardly be attempted 'in-vivo' since 'in-vivo' phonation presents itself as an indivisible entity which can not be split up into distinct separable and controllable events. So although 'in-vivo' observations are a benchmark for the phenomena under study [10, 11, 6, 4, 7, 9], mechanical replicas with increasing degrees of complexity are developed in order to validate theoretical models [12, 13, 14, 15, 16, 17, 18]. In [14] the initial aperture is varied from 0 up to 2 mm, while the 'in-vitro' replica is an asymmetric geometry consisting of one 'in-vitro' vocal fold placed in a 9 cm channel so that a rectangular glottis is obtained. In addition, it was aimed to study the vocal fold mucosa and therefore the vocal fold body was rigid so that the influence of mechanical parameters such as the stiffness could not be studied.

The current paper presents an experimental study of the influence of varying initial aperture and mechanical properties on predicted oscillation onset pressure and oscillation frequency for weak and strong acoustic coupling

Received 1 September 2010,
accepted 12 January 2011.

since recent modelling studies point out its importance [19, 20]. Next, particular attention is given to the estimation of model parameters from experimental observations. Finally, theoretical predictions are validated on a deformable replica.

1. Theoretical symmetrical vocal fold model

Theoretical modeling of self-sustained oscillations of a vocal folds replica is performed by using a theoretical symmetrical two mass model inspired on the work presented in [3, 21] and briefly detailed in Appendix A1. Each of the vocal folds is modeled as a reduced spring-mass-damper system with two degrees of freedom driven by the pressure difference across the masses. The applied models describing glottal airflow, vocal folds mechanics and acoustic interaction with an upstream and downstream pipe, representing the trachea and the vocal tract, are severe simplifications of the fluid-structure interaction in the larynx during human voiced sound production.

The airflow model relies on the assumption of a quasi-steady inviscid and incompressible flow within the glottis corrected for some major viscous effects, firstly in case of small glottal apertures and secondly to account for flow separation and the formation of a jet [22]. The main parameters related to the flow model are the time evolution of the driving subglottal pressure $P_u(t)$, the time evolution of the glottal cross sectional area $A(x, t)$, where x indicates the flow direction, and the position of the flow separation point. Liljencrants 'ad-hoc' separation criterion is applied to define a moving separation point in the diverging downstream part of the constriction at a position corresponding to the glottal area $A_s = c_s A_{min}$, with A_{min} the minimum constriction area and $c_s \geqslant 1$ an 'ad-hoc' separation constant.

The vocal folds mechanics is modeled as a symmetrical low order model in which each vocal fold is represented by two identical masses [3, 21]. The two mass model describes the movement of the two masses perpendicular to the flow direction assuming a rectangular glottal area with fixed width w. The geometrical description could thus be given in terms of the center aperture of the glottal area, i.e. $h_c = A/w$. Except geometrical parameters as e.g. measured initial aperture h_c^0 and subglottal pressure P_u expressing the coupling with the flow model, the main parameters required in the mechanical model are mass m, spring stiffness K, coupling stiffness K_c between the two masses, damping R and critical aperture threshold h_{crit} applied in the discrete collision model. Notice that in the current model the collision model was triggered on the glottal aperture, independent from the impact velocity. Whenever collision was detected following the criterion $h_c < h_{crit}$ the values of K and R are increased to $K = 4K$ and $R = R + 2\sqrt{Km}$. The fixed collision threshold h_{crit} is commonly set to 0.02 mm. This threshold value is validated to be suitable in case the assumption of a rectangular area with fixed length was made and consequently h_c fully described the geometry [23]. The two masses have the same mechanical parameters K, R and m as systematically depicted in Figure A1.

Table I. Theoretical model input parameters.

Flow model parameter set $\{P_u(t), h_c^0, c_s\}$	
$P_u(t)$	(subglottal) upstream pressure [Pa]
h_c^0	initial aperture [mm]
c_s	'ad-hoc' separation constant [-] (fixed at 1.2)
Mechanical model parameter set $\{h_{crit}, m, K, R, \gamma\}$	
h_{crit}	'ad-hoc' critical aperture threshold [mm] (fixed at 0.02)
m	mass [kg]
K	spring stiffnes [kg/s^2]
R	damping [kg/s]
γ	coupling parameter [–]
Acoustical model parameter set $\{L_d\}$	
L_d	downstream pipe length [cm]

Commonly, the coupling stiffness is 'ad-hoc' defined as $K_c = 0.5 \cdot K$ [3, 21]. In the following, we describe the relationship between stiffness K and coupling stiffness K_c by introducing an additional model parameter γ, labelled coupling parameter, defining a linear relationship as $\gamma = \frac{K_c}{K}$. Recall that introducing the parameter γ is consistent with a fixed time-delay between two masses in a delayed one-mass model [21].

Acoustical coupling between the vocal folds and a uniform downstream pipe, representing the vocal tract in the model, is important when the acoustical resonance frequencies of the pipe and the oscillation frequency are close. Therefore, the importance of acoustical coupling with a downstream pipe depends on its length L_d [24, 21, 19, 20].

Required model input parameters are summarised in Table I. Except for the 'ad-hoc' separation constant c_s and the fixed critical aperture threshold $h_{crit} = 0.02$ their values are sought to be determined from experimental observations.

2. 'In-vitro' setup

The experimental setup and deformable 'in-vitro' vocal fold replica are described in sections 2.1 and 2.2 and illustrated in Figure 1. Table II gives an overview of the experimentally varied and observed parameters as explained in the following sections.

2.1. Experimental setup

The deformable replica detailed in section 2.2 is mounted in an experimental setup in order to generate self-sustained oscillations and to measure characteristic oscillation quantities. An air supply is connected to a pressure tank of 0.75 m^3 filled with acoustical foam, enabling to impose an airflow through the deformable replica. The pressure

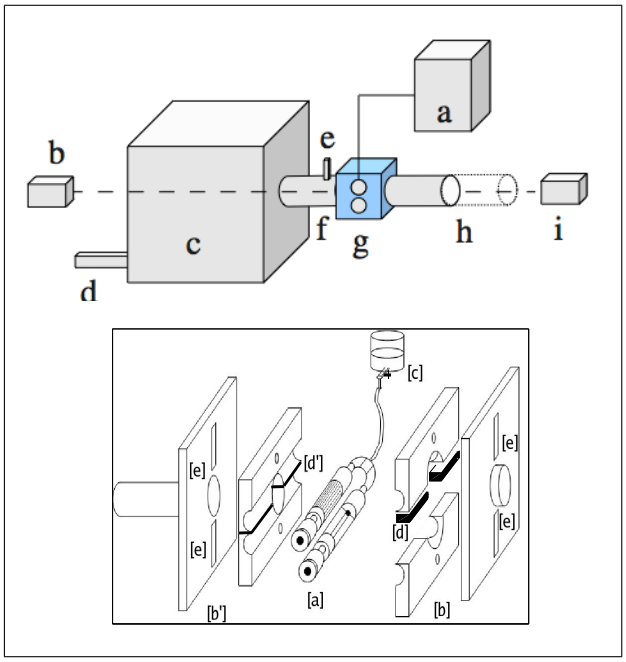

Figure 1. (a) Schematic overview of experimental setup with [a] water column with controllable height connected to the vocal fold replica [g] detailed in (b) with [h] downstream pipe of variable length L_d and upstream pipe [f] with pressure tap to measure the upstream pressure [e] and which is mounted to the pressure reservoir [c] to which air is supplied [d]. The deformation of the replica is measured by means of a laser beam (dashed line) emitted from source [b] and brought to focus on the light sensitive sensor [i]. (b) Schematic representation of the deformable replica. Latex tubes [a] are connected to water column [c] enabling to impose the internal pressure P_{in}. Each latex tube is mounted in a metal block [b,b'] by means of fixation screws [e]. The initial geometrical configuration in absence of airflow was characterized by the center aperture h_c^0. h_c^0 is varied 1) by imposing internal pressure P_{in} and 2) by inserting a set of shims [d] between the outer parts of the upper and lower portion of the mounting block. In absence of shims the aperture is minimal [d'].

upstream from the replica, P_{up}, is measured by means of a dynamic piezo-resistive pressure transducer (Kulite XCS-093) positioned in a pressure tap of 0.4 mm diameter in an upstream uniform pipe with diameter 25 mm and fixed length of 3.5 cm. The pressure transducer is calibrated against a water manometer with an accuracy of 1 Pa. The attached downstream circular pipes, forming the artificial vocal tract, have a fixed internal diameter of 25 mm and variable length L of 49.5, 28.6 or 18.5 cm respectively. In the following, the downstream pipes are indicated by subscripts 50, 28 and 18. The corresponding first f_{ac}^1 and second f_{ac}^2 acoustical resonance frequencies for upstream and downstream pipes are given in Table III.

The instantaneous replica aperture $h_c(t)$ is observed by means of a laser beam (635 nm) passing through the replica and brought to focus on a light sensitive sensor (BPW 34). The optical laser system is calibrated to relate the transmitted light intensity of the original beam to the center distance h_c between the two tubes at the center of the aperture area. This way time-varying center apertures $h_c(t)$ up to 8 mm are measured with an accuracy of 0.01 mm. The measured aperture $h_c(t)$ is related to the open area by assuming a uniform rectangular open area with fixed length $w = 25$ mm being the constant width of the replica exposed to the airflow, i.e. $A_c(t) = h_c(t)w$. The assumption of a rectangular area, $A_c(t) = h_c(t)w$, and hence of a uniform displacement is validated for the replica under study by means of a camera imaging the open area [23]. This way the deformation of the replica due to the interaction with airflow is observed while increasing the upstream airflow from 0 up to 3000Pa in order to detect the required minimum pressure P_{on} for which self-sustained oscillation occurs and the associated oscillation frequency f. The aperture measured for $P_{up} = 0$ corresponds to the imposed initial aperture h_c^0. In addition, measurement of the deformation $h_c(t)$ due to acoustical excitation is performed to determine the mechanical frequency response of the replica [25, 21].

Table II. Experimentally controlled and observed variables.

Controlled parameters	
P_{up}	upstream air pressure [Pa]
P_{in}	internal water pressure in latex tubes [Pa]
h_c^0	initial aperture [mm] (by means of shim d)
L	upstream circular pipe length [cm]
Observed parameters	
P_{on}	minimum P_{up} required for self-sustained oscillation [Pa]
f	oscillation frequency [Hz]

Table III. First and second acoustical resonance frequencies $f_{ac}^{1,2}$ for upstream pipe length 3.5 cm (L_{up}) and assessed downstream pipe lengths of 18.5 (L_{18}), 28.6 (L_{28}) and 49.5 cm (L_{50}).

L [cm]	L_{up}	L_{18}	L_{28}	L_{50}
f_{ac}^1 [Hz]	2429	460	297	172
f_{ac}^2 [Hz]	4857	919	594	344

2.2. Deformable replica

The deformable replica, illustrated in Figure 1b, mimics the deformable physiological vocal fold structure by two connected latex tubes (Piercan Ltd.), with density 0.98 g/cm^3 and Young's modulus 0.35 MPa, of 11 mm diameter and 0.3 mm thickness. The tubes are mounted on two metal cylinders with diameter 12 mm for which the metal was removed over half the diameter for a length of 40 mm. The latex tubes are filled with water supplied through a central duct of 3 mm diameter connected to a water column. The height of the water column, and so internal pressure P_{in} in the latex tubes, is controllable. The latex tubes are fixated in a metal block in order to prevent leakage. Increasing or decreasing the internal pressure P_{in} by lifting or lowering the water column implies a change in initial aperture between the two tubes and consequently the two parameters are related in a unique way. In order to vary

the initial aperture and P_{in} in a non-unique way an equal set of uniform rectangular metal blocks with fixed length (12 mm), fixed width (16 mm) and variable thickness d, further referred to as shims d, can be inserted at the outer borders between the upper and lower portion of the replica separating both latex tube holders to a user controlled extent. This way, the initial center aperture at rest h_c^0 is arbitrarily varied from complete closure $h_c^0 = 0$ to a maximum aperture of $h_c^0 = 10$ mm. In the present work, shims of thickness $d = 0.0$ (absence of shims), $d = 0.5$ and $d = 1.0$ mm are used in order to significantly vary the initial aperture of the replica and to experimentally explore a considerable region in the (P_{in}, h_c^0) parameter space. Note that by using three different shims d, three different h_c^0 are associated with each P_{in}. For each shim d, the internal pressure is gradually increased in steps of 500 Pa from 500 Pa up to complete closure, *i.e.* $h_c^0 = 0$. The resulting variation of $h_c^0(P_{in}, d)$ is illustrated in Figure 2 for the 3 used shims d.

Closure of the replica (h_c^0=0 mm) occurred at P_{in} = 8000, 9500 and 11000 Pa in case of shims 0.0, 0.5 and 1.0 mm, respectively. For all imposed P_{in}, so $P_{in} = c$ with c a constant, the use of different shims d introduces a variation of $h_c^0(P_{in} = c, d)$ corresponding to about 16% at P_{in} = 500 Pa which increases up to 50% upon closure. The dashed line represents a linear fit of $h_c^0(P_{in}, d)$ from which the deformation $\Delta h_c^0(d)$ is obtained. The initial measured center aperture h_c^0 determines the geometry in the model since a rectangular open area is assumed to model the glottal area.

Recall that varying P_{in} by lifting or lowering the water column changes the mechanical properties and the total mass of the latex tubes. For all assessed configurations (d, P_{in}), the total mass is estimated to be less than 3 g based on geometrical considerations.

3. Experimental and model parameters

Except for 'ad-hoc' parameters which are inherent to the model, such as c_s and h_{crit}, comparison of measured and predicted quantities requires input parameters of the theoretical model to be determined from experimentally imposed quantities as shown in Table IV.

The sought relationship is straightforward in case of parameters required in the flow and acoustic model. The measured upstream pressure P_{up} corresponds to the driving pressure P_u in the theoretical model. The initial aperture corresponds to h_c^0 and the experimentally assessed downstream pipe length L corresponds to the model parameter L_d. The mechanical model parameters m, K, R and γ on the other hand, need to be estimated from the measu red mechanical resonance properties of the replica imposed by P_{in}. In addition, the Young's modulus E of the replica can be estimated from the measured frequency response and deformation estimated by the slope of $h_c^0(P_{in}, d)$ as shown in Figure 2. Therefore, parameter estimation from the measured mechanical frequency response is detailed in the next subsections.

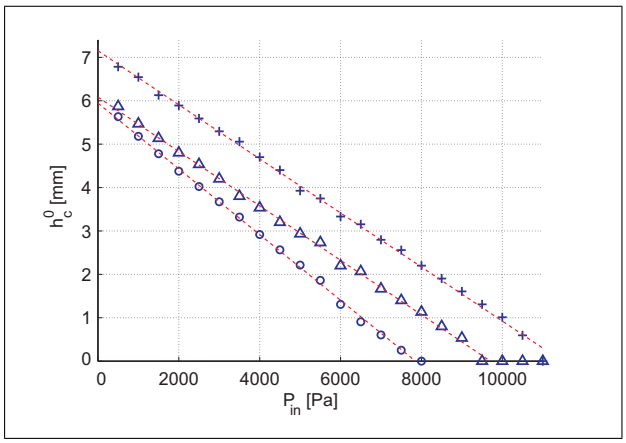

Figure 2. Measured initial center apertures $h_c^0(P_{in}, d)$ for shims $d = 1.0$ (+), $d = 0.5$ (△) and $d = 0.0$ (∘) mm as function of P_{in}. The dashed lines indicated a linear fit for each shim set with slope -0.00062, -0.00063 and -0.00076 for shims 1.0, 0.5 and 0.0 respectively.

Table IV. Relationship between theoretical model input parameters and experimental control parameters is either straightforward (direct) or obtained from the measured frequency response (F, Q) as function of P_{in}. Recall that both c_s (flow) and h_{crit} (mechanical) are 'ad-hoc' model parameters for which no relationship with experimental quantities is sought and they are therefore omitted in the table.

	theoretical	experimental	relation
flow	$\{P_u(t), h_c^0\}$	$\{P_{up}(t), h_c^0\}$	direct
mechanical	$\{m, K, R, \gamma\}$	$\{P_{in}\}$	(F, Q)
acoustic	$\{L_d\}$	$\{L\}$	direct

3.1. Estimation of stiffness K, damping R and mass m

The mechanical resonance characteristics inform on the resonance frequencies F, i.e. the resonance peaks in the frequency domain ω, and associated quality factors Q [25]:

$$Q = \frac{F}{\Delta F_{-3dB}}, \tag{1}$$

with ΔF_{-3dB} the -3 dB bandwidth. The obtained experimental parameters F_i and Q_i, with peak index i, correspond to the sought quantities $\omega_i = 2\pi F_i$ and Q_i in the mechanical equations of low-order physical vocal fold models. The effective mass μ_i is than estimated for each resonance peak by fitting the magnitude of the mechanical response, $|C(\omega)|$, in the neighborhood of the ith peak as

$$\left|C(\omega)\right| = \left.\frac{\frac{Q_i}{\omega_i^2}\frac{1}{|\mu_i|}}{\sqrt{1 + 4Q_i^2\left(\frac{\omega-\omega_i}{\omega_i}\right)^2}}\right|_{\omega\approx\omega_i} \approx \frac{Q_i}{\omega_i^2\mu_i}. \tag{2}$$

The vibrating mass portion is approximated as $m \approx \mu_i \times w \times l$ with $w = 0.024$m the uniform width of the glottal replica and $l = 0.008$m the length of the replica in contact

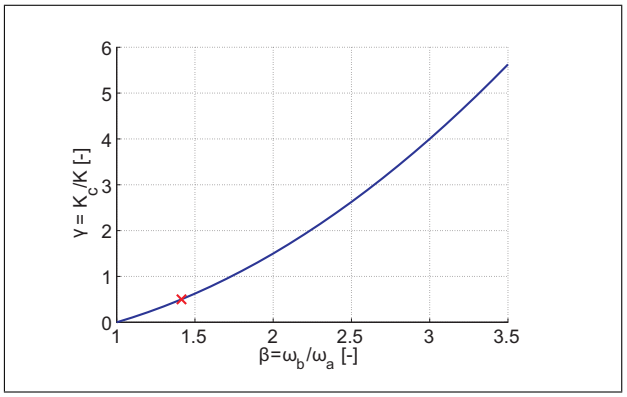

Figure 3. The model coupling parameter $\gamma(\beta) = \frac{1}{2}\left[\beta^2 - 1\right]$ with $\beta = \frac{\omega_b}{\omega_a} > 1$ relates K and K_c as expressed in equation (5). The common 'ad-hoc' model value $\gamma(\beta = \sqrt{2}) = 0.5$ (×) is indicated as well [3, 21].

with the fluid, so that $w \times l$ represents the effective surface on which the pressure acts. The stiffness K and the damping R are obtained as

$$K \approx m\omega_i^2 \quad R \approx m\frac{\omega_i}{Q_i}. \tag{3}$$

The stiffness K increases as the resonance frequency increases. A small Q_i value or large bandwidth corresponds to a large damping R_i of the resonance peak and vice-versa.

3.2. Estimation of the coupling parameter γ

The coupling stiffness K_c is commonly 'ad-hoc' fixed to half the spring stiffness K, i.e. $K_c = 0.5 \cdot K$ or $\gamma = 0.5$ [3, 21]. In order to relate K_c to the measured mechanical response and therefore to avoid a fixed 'ad-hoc' value, the following relations are taken into account [26]:

$$\omega_a = \sqrt{\frac{K}{m}}, \quad \omega_b = \sqrt{\frac{K + 2K_c}{m}}, \tag{4}$$

with $\omega_a < \omega_b$ two measured mechanical resonance frequencies for a given P_{in}. From equation (4) follows immediately:

$$\gamma = \frac{K_c}{K} = \frac{1}{2}\left[\frac{\omega_b^2}{\omega_a^2} - 1\right] = \frac{1}{2}\left[\beta^2 - 1\right], \tag{5}$$

with β defined as

$$\beta = \frac{\omega_b}{\omega_a} > 1. \tag{6}$$

The impact of the quadratic relationship $\gamma(\beta)$ on the range of estimated γ values is illustrated in Figure 3.

The common 'ad-hoc' value $\gamma = \gamma(\beta = \sqrt{2}) = 0.5$ corresponding to $\omega_b = \sqrt{2}\omega_a$ is indicated as a benchmark. As will be shown further, the illustrated β-set, $\beta \in]1\ 3.5] \Rightarrow \gamma \in]0\ 5.6]$, is relevant with respect to the performed 'in-vitro' experiments.

3.3. Estimation of Young's modulus E

The Young's modulus E_L, where the subscript L indicates that the Young's modulus is associated with the mechanical resonance frequency ω_L, is estimated from the stiffness as:

$$E_L(\omega_L) = \frac{K}{\Delta h_c^0}, \tag{7}$$

with mass m, stiffness $K = m\omega_L^2$ and Δh_c^0 denoting the deformation induced by varying P_{in} as pointed out in section 2.2 and Figure 2.

4. Experimental results and discussion

Parameters estimated from the measured mechanical frequency response are presented in subsection 4.1. Next, the measured minimum pressure required for self-sustained oscillation of the replica P_{on} and corresponding oscillation frequency f are discussed in subsection 4.2.

4.1. Mechanical frequency response and parameter estimation

The mechanical frequency response of the replica is determined by the internal pressure P_{in}. For each P_{in}, two or three mechanical resonance frequencies F and associated bandwidths Q are measured. It is shown in Figure 2 that due to the use of three different shims d, three initial apertures h_c^0 are associated with each assessed P_{in} value. Consequently, mechanical resonance properties F and Q can be expressed as function of P_{in} or plotted against the three corresponding $h_c^0(P_{in}, d)$. Mechanical features F and Q are expressed as function of h_c^0 rather than P_{in} since h_c^0 is a model input parameter whereas P_{in} is an experimental control quantity used to vary mechanical properties in a quantitative and controllable way. Obtained F and Q values are shown in Figure 4 for $h_c^0(P_{in}, d)$ obtained for shim $d = 1.0$ mm.

Figure 5 gives an overview of resulting $F(h_c^0(P_{in}, d))$ for all three assessed shims $d = 0.0$, $d = 0.5$ and $d = 1.0$ mm. For clarity the maximum measured aperture for each shim as well as the relevant P_{in}-range and P_{in}-values associated with maximum aperture and complete closure are indicated. Consequently, 3 distinct mechanical feature sets, $(F, Q)(h_c^0)$, are experimentally assessed while h_c^0 is maintained fixed.

For each resonance peak, the mass m is estimated from the mechanical frequency response following eq. 2. Resulting mass estimations are illustrated in Figure 6 for the first and second resonance frequencies.

As for F and Q, the mass estimation m associated with the geometrical model parameter h_c^0 depends on the used shim d. The estimated mass values ($m < 1$ g) are smaller than the geometrical maximum mass estimation of 3 g.

The model parameters K and R are analytically obtained from the set (m,F,Q) and depend therefore on P_{in} as well as $h_c^0(P_{in}, d)$. Furthermore, from Figure 5, $F_1 \approx 106$

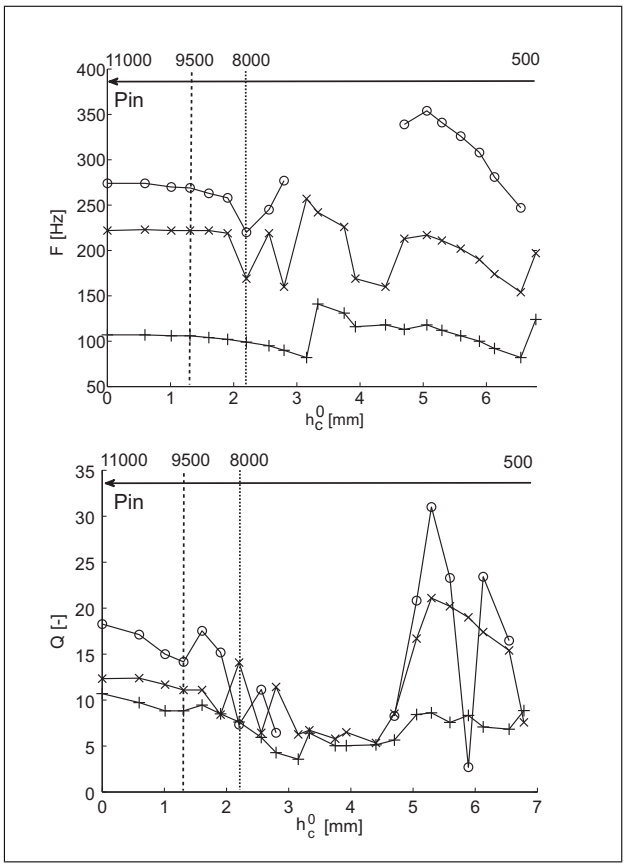

Figure 4. First (+), second (×) and third (∘) mechanical resonance frequencies $F(P_{in})$ and associated quality factors $Q(P_{in})$. The relationship $F(h_c^0)$ and $Q(h_c^0)$ is obtained from $h_c^0(P_{in}, d)$ as shown in Figure 2. This is illustrated for shim $d = 1.0$ mm. The dashed lines illustrate P_{in} values associated with complete closure in case of shim $d = 0.5$ (9500 Pa) and $d = 0.0$ (8000) Pa.

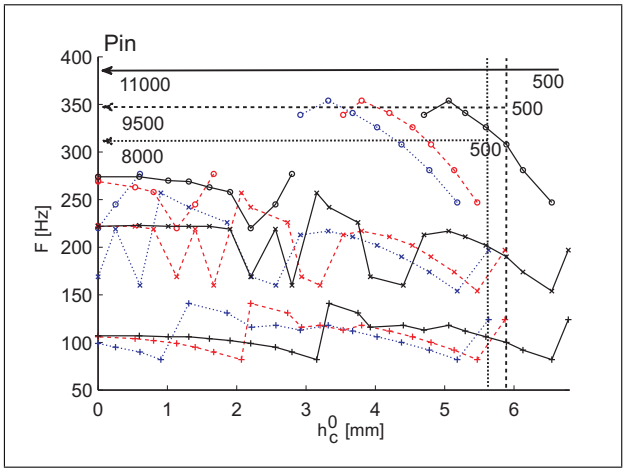

Figure 5. First (+), second (×) and third (∘) mechanical resonance frequencies $F(h_c^0)$, using $h_c^0(P_{in}, d)$, for each of the shims $d = 0.0$ (dotted), $d = 0.5$ (dashed) and $d = 1.0$ (full) mm. The P_{in} range from maximum aperture at $P_{in} = 500$ (vertical dashed lines) up to closure is indicated for each of the 3 shims d.

and $F_2 \approx 222$ Hz are seen to be rough estimates of the magnitude of the first and second mechanical resonance frequencies for all 3 shims d. For both frequencies the corresponding Young's modulus $E(F_{1,2})$ is qualitatively estimated by applying eq. 7 with thedeforma tion $\Delta h_c^0(d)$ taken from the linear fit of $h_c^0(P_{in}, d)$ shown in Figure 2. Resulting Young's modulus estimations are shown in Figure 7.

The estimated Young's modulus for shims 1.0 and 0.5 almost overlap since the slopes of the linear fit, and so the deformation, for shims $d = 1.0$ and $d = 0.5$ are in

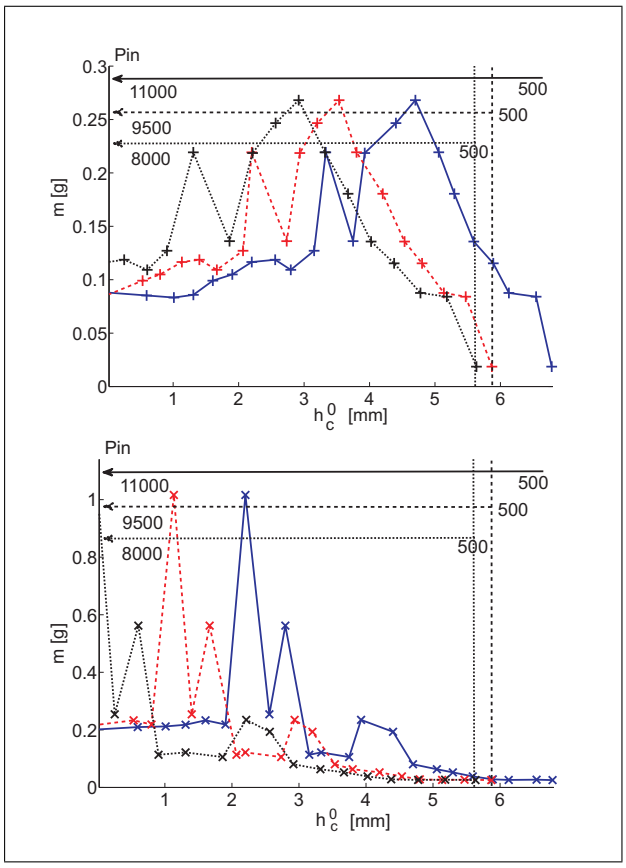

Figure 6. Mass estimation m as a function of the initial aperture h_c^0 estimated on a) first F_1 and b) second F_2 mechanical resonance frequency for each of the shims: 0.0 (dotted), 0.5 (dashed) and 1.0 (full) mm.

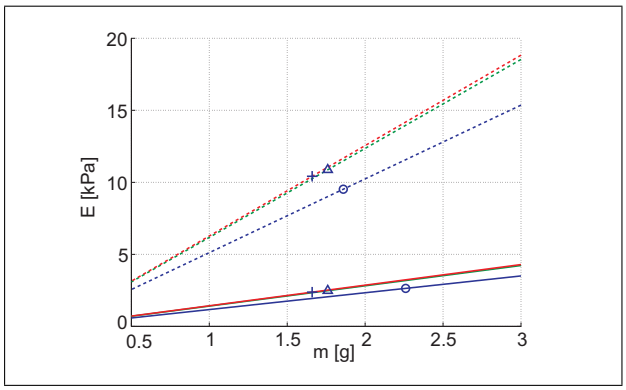

Figure 7. Estimation of the Young's modulus $E(m)$ for resonance frequencies of 106 Hz (straight lines) and 222 Hz (dashed lines) and linear fits of $h_c^0(P_{in}, d)$ as shown in Figure 2 for each of the shims: $d = 1.0$ (+), $d = 0.5$ (△) and $d = 0.0$ (∘).

a close match. The estimated Young's modulus for shim $d = 0.0$ mm is smallest due to the large deformation, *i.e.* large slope magnitude as shown in Figure 2. Since the stiffness K increases linear with increasing m, the estimated Young's modulus increases linearly with m. The retrieved values are within the order of magnitude reported for 'in-vivo' estimations [10, 11], although reported 'in-vivo' values vary significantly (1-20 kPa). Recall that both the magnitude of the gathered resonance frequencies as well as the number of resonances peaks on the 'in-vitro' measured mechanical resonance frequencies are relevant with respect to 'in-vivo' observations [4].

Acoustical resonance frequencies f^{ac} summarised in Table III of the upstream pipe of 3.5 cm are much larger than mechanical resonance frequencies, *i.e.* $f^{ac} > 400$ Hz, so that upstream acoustical coupling can be neglected for the current setup [24]. For the downstream pipes acoustical coupling is important for L_{50} and L_{28} and not for L_{18}. In particular $f_{50}^{ac,1} = 172$, $f_{28}^{ac,1} = 297$ and $f_{50}^{ac,2} = 343$ Hz are within the range of mechanical resonance frequencies.

The mechanical coupling parameter $\gamma(\beta(h_c^0))$ is estimated from the ratio of resonance frequencies β as outlined in section 3.2. Following equation (6) three β's, *i.e.* $\beta_{1,2,3}$, can be defined from the experimentally observed resonance frequencies,

$$\beta_1 = \frac{F_2}{F_1}, \quad \beta_2 = \frac{F_3}{F_2}, \quad \beta_3 = \frac{F_3}{F_1}. \tag{8}$$

Obviously, if no third resonance frequency F_3 is experimentally observed, only β_1 can be quantified. The same way as for F and Q, for each assessed shim d, firstly $\beta(h_c^0)$ and next $\gamma(h_c^0)$ is deduced for the mechanical resonance frequencies as illustrated for shim $d = 1.0$ mm in Figure 8. Figure 9 illustrates $\gamma(h_c^0(P_{in}, d))$ for all 3 shims d.

This way, all mechanical model parameters (except the 'ad-hoc' collision threshold h_{crit}) are estimated from experimental data and no 'ad-hoc' parameter, corresponding to $\gamma = 0.5$, is needed to determine the coupling stiffness. Moreover experimentally estimated γ values cover the domain shown in Figure 3.

4.2. Auto-oscillation features

Experimentally observed upstream pressures at self-sustained oscillation onset $P_{on}(h_c^0)$ and associated oscillation frequencies $f(h_c^0)$ are presented in Figure 10 and 11 for each of the 3 assessed downstream pipes. The experimental observed P_{on} and oscillation frequencies f depend on the initial center aperture h_c^0, the mechanical properties imposed by P_{in} and the acoustical coupling with the downstream pipe of length L. Based on the initial center aperture h_c^0, two oscillation regions, further labelled I and II, are experimentally identified for $h_c^0 < 2.2$ mm and $h_c^0 > 4$ mm respectively. No vibration was observed for values of h_c^0 in between the two oscillatory regimes. The main characteristics of both oscillation regions are summarised in Table V.

The first ($h_c^0 < 2.2$ mm) oscillation region I, characterised by $1000 < P_{on} < 2500$ Pa and $145 < f < 270$ Hz, is experimentally observed for all assessed downstream pipes and shims d. Nevertheless, observed P_{on} and

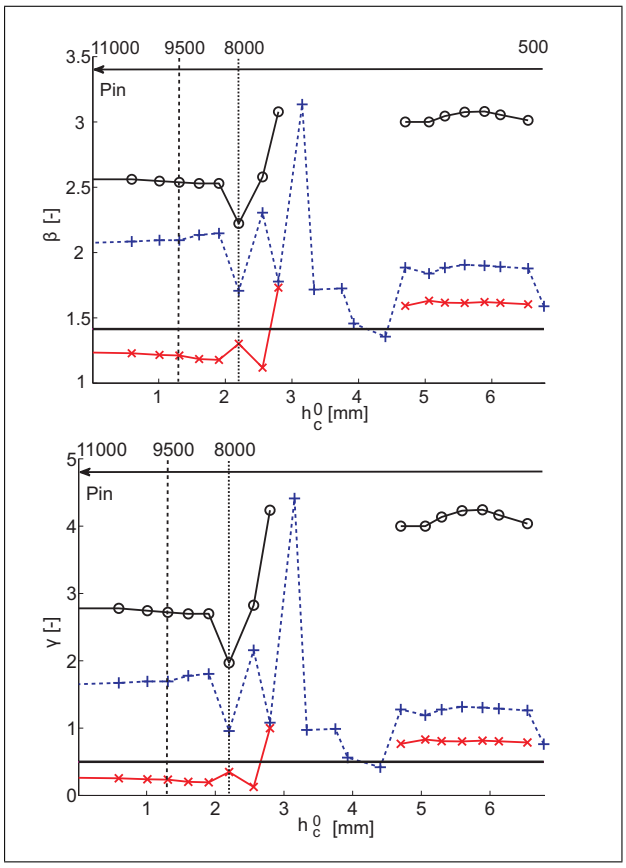

Figure 8. a) $\beta(h_c^0)$ for shim $d = 1.0$ mm. β_1 (+), β_2 (×) and β_3 (∘) derived as F_2/F_1, F_3/F_2 and F_3/F_1 respectively. b) $\gamma(h_c^0)$ for shim $d = 1.0$ mm. $\gamma(\beta_1)$ (+), $\gamma(\beta_2)$ (×) and $\gamma(\beta_3)$ (∘). The straight full line indicates $\gamma = 0.5$ corresponding to $\beta = \sqrt{2}$ depicted in (a). The dashed lines illustrate P_{in} values associated with closure for shim $d = 0.5$ (9500 Pa) and $d = 0.0$ (8000) Pa.

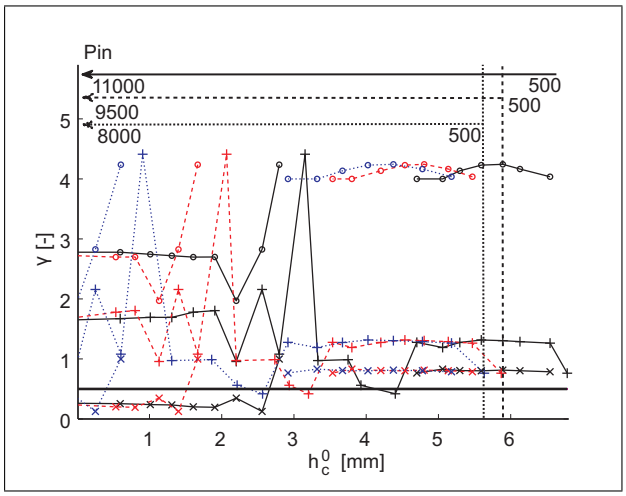

Figure 9. $\gamma(h_c^0)$ for each of the shims 0.0 (dotted), 0.5 (dashed) and 1.0 (full) mm and $\gamma(\beta_1)$ (+), $\gamma(\beta_2)$ (×) and $\gamma(\beta_3)$ (∘). The straight full line indicates $\gamma = 0.5$ in accordance with $\beta = \sqrt{2}$ depicted in Figure 8a. The P_{in} range from maximum aperture ($P_{in} = 500$) up to closure is indicated for each of the shims.

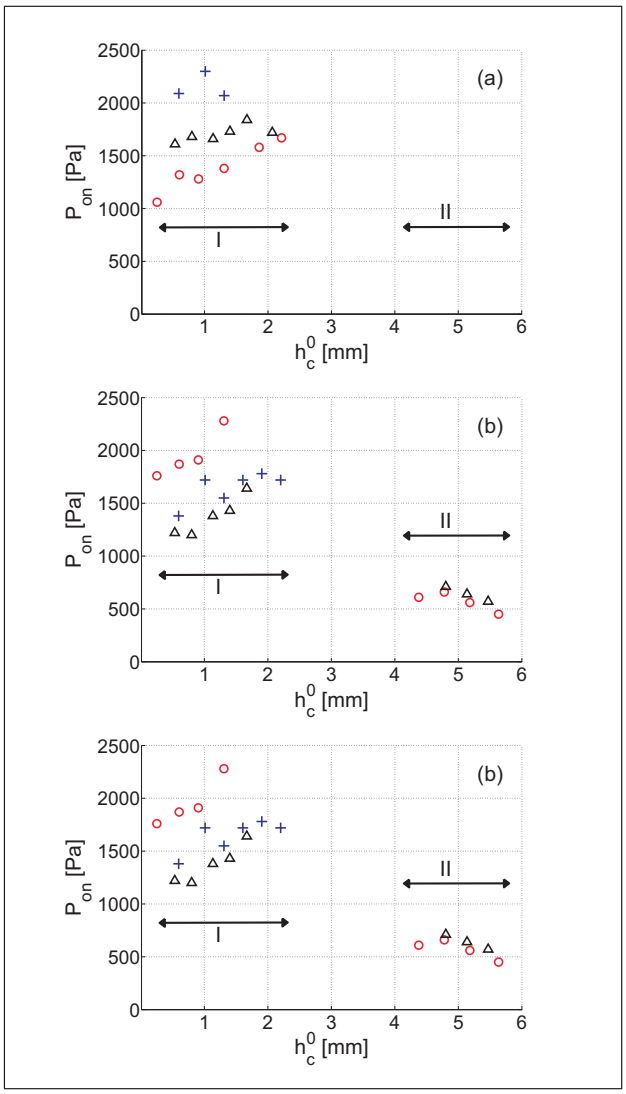

Figure 10. The measured oscillation onset pressure P_{on} as a function of the initial aperture h_c^0 for different downstream resonators of length L and shims, *i.e.* $d = 1.0$ (+), $d = 0.5$ (△) and $d = 0.0$ (∘) mm. I and II indicate the first ($h_c^0 < 2.2$ mm) and second ($h_c^0 > 4$ mm) oscillation region, respectively. (a) L = 49.5 cm, (b) L = 28.6 cm, (c) L = 18.5 cm.

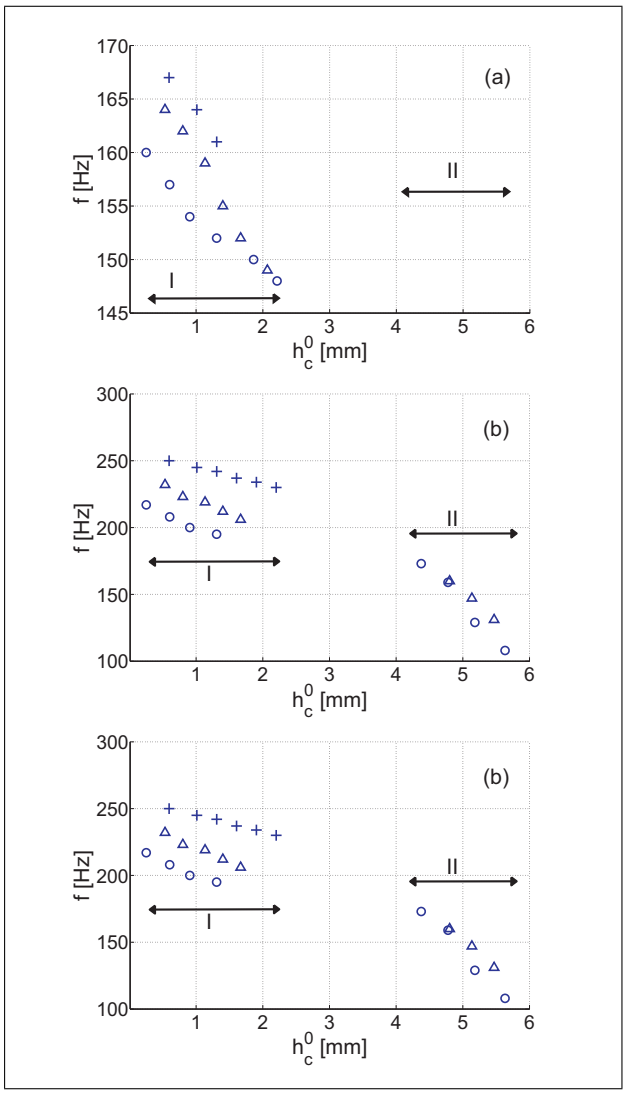

Figure 11. The measured oscillation frequencies f as function of the initial aperture h_c^0 for different downstream resonators of length L and shims, i.e. 1.0 (+), 0.5 (△) and 0.0 (∘) mm. I and II indicate the first ($h_c^0 < 2.2$ mm) and second ($h_c^0 > 4$ mm) oscillation region, respectively. (a) L = 49.5 cm, (b) L = 28.6 cm, (c) L = 18.5 cm.

Table V. Main observations for oscillation regions.

osillation region	I	II
h_c^0 [mm]	$h_c^0 < 2.2$	$h_c^0 > 4$
P_{in} [Pa]	$P_{in} > 5000$	$P_{in} < 2000$
P_{on} [Pa]	$1000 < P_{on} < 2500$	$400 < P_{on} < 700$
f [Hz]	$145 < f < 270$	$100 < f < 170$

f values for a same initial aperture value h_c^0 obtained with different shims d vary significantly, e.g. $1400 < P_{on} < 2300$ Pa for $h_c^0 \approx 1$ mm. The observed variation results from the large variation of mechanical properties associated with different shims d when a fixed initial aperture in the region $h_c^0 < 2.2$ mm is considered, e.g. $h_c^0 \approx 1$ mm corresponds to a variation of $6500 < P_{in} < 10000$ Pa in Figure 5.

The second ($h_c^0 > 4$ mm) oscillation region II, characterised by $400 < P_{on} < 700$ Pa and $100 < f < 170$ Hz, is experimentally observed for L_{28} and L_{18} in case of shims $d = 0.0$ and $d = 0.5$ mm and is absent for L_{50} and shim $d = 1.0$ mm. The close agreement (< 10 %) in the observations for shims 0.0 and 0.5 mm in this second region is due to the small differences in mechanical properties and in h_c^0 (< 5%) as seen in Figure 2. Therefore, mechanical properties for a given initial aperture $h_c^0 > 4$ for $d = 0.0$ and $d = 0.5$ mm closely match (see Figure 5).

The influence of acoustical coupling with the downstream pipe on the measured oscillation frequencies f is observed in the first oscillation region ($h_c^0 < 2.2$ mm) in case the longest assessed pipe length L_{50} is used. The first acoustical resonance frequency, equal to 170 Hz reported

Table VI. Applied parameter estimations for $\gamma(\beta_1)$, $\gamma(\beta_2)$, $m(F_1)$ and $m(F_2)$ for oscillation regions I and II. Values in bold result in a qualitative good estimation of the onset threshold pressure.

osillation region h_c^0 [mm]	I $]h_{crit}$ 2.2]	II [4 6]
$\gamma(\beta_1)$ [-]	**0.25**	0.80
$\gamma(\beta_2)$ [-]	1.69	**1.29**
$m(F_1)$ [g]	**[0.08 0.22]**	[0.27 0.01]
$m(F_2)$ [g]	[0.1 1.02]	**[0.24 0.02]**

in table III, is seen to impose the oscillation frequency f. The observed strong acoustical coupling is in agreement with findings reported in [24]. For shorter pipe lengths acoustical coupling is weaker and does not influence f. In case of weak acoustical coupling, the observed oscillation frequencies $180 < f < 280$ approach F_2 and F_3 in the first oscillation region. So, the third and second mechanical resonance frequencies are favored due to the large damping for F_1 as seen from the low value of Q_1.

In general, the measured oscillation features P_{on} and f are shown to depend on initial mechanical (F, Q imposed by P_{in}), geometrical ($h_c^0(d, P_{in})$) and acoustical coupling conditions with the downstream pipe (L).

5. In-vitro validation and discussion

In order to validate the model (and the parameter estimation) predicted oscillation onset pressure thresholds are compared to experimentally observed values P_{on}. Experimental and simulated P_{on} as function of initial center aperture $h_c^0 > h_{crit}$ are presented in Figure 12. Simulations are performed with model parameters estimated as outlined in section 3 and the coupling stiffness derived from β_1 and β_2. Only values $h_c^0 > h_{crit}$ del validation in order to avoid the influence of the 'ad-hoc' parameter h_{crit} mm used in the discrete collision model.

Depending on the shim d and initial aperture h_c^0 best simulation results are obtained with either $\gamma(\beta_1(h_c^0))$ or $\gamma(\beta_2(h_c^0))$. In general, predictions with $\gamma(\beta_1(h_c^0))$ provides qualitative good predictions for the first oscillation region I, whereas predictions with $\gamma(\beta_2(h_c^0))$ results in qualitatively good estimations for the second oscillation region II. With respect to the used shim d qualitat with $\gamma(\beta_2(h_c^0))$, for shim $d = 0.5$ with $\gamma(\beta_2(h_c^0))$ and $\gamma(\beta_1(h_c^0))$ and for shim $d = 1.0$ with $\gamma(\beta_1(h_c^0))$. Corresponding γ estimations, for which an overview is given in Table VI, vary in the range $0.25 < \gamma < 1.69$ compared to $\gamma = 0.5$ for the fixed 'ad-hoc' value. Consequently, estimated coupling stiffness range from 0.5 up to 3.38 times the fixed 'ad-hoc' value. For coresponding estimations of the mass m.

The model outcome with the coupling parameter estimated from measured values presents several satisfying qualitative features with respect to the measured P_{on} values: 1) in terms of the retrieved two distinct oscillation regions for small and large initial apertures respectively, 2) in terms of the estimated variation of P_{on} with respect to

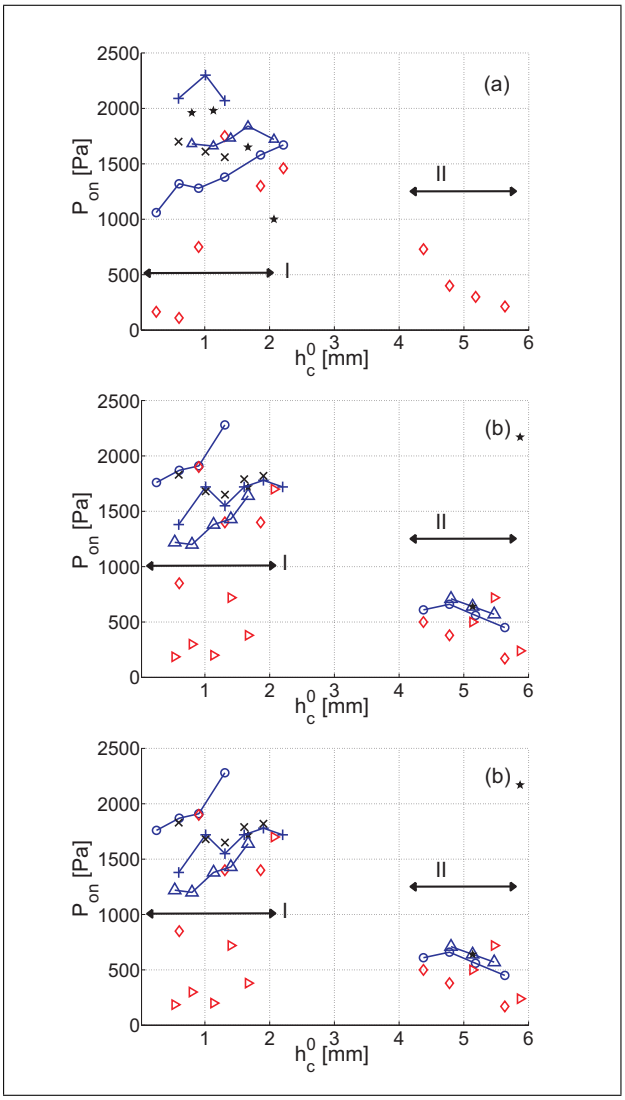

Figure 12. Measured, shim $d = 0.0$ ($\circ - \circ$), $d = 0.5$ ($\triangle - \triangle$), $d = 1.0$ ($+ - +$), and predicted threshold pressure P_{on} as a function of the initial aperture h_c^0 for different downstream resonators of length L. Predictions are obtained with the coupling stiffness derived from β_1 ($\bigstar$ for shim 0.5, $\times$ for shim 1.0 - black) and β_2 ($\Diamond$ for shim 0.0, $\triangleright$ for shim 0.5 - red). I and II indicate the first ($h_c^0 < 2.2$ mm) and second ($h_c^0 > 4$ mm) oscillation region, respectively. (a) L = 49.5 cm, (b) L = 28.6 cm, (c) L = 18.5 cm.

variation of mechanical properties for a given initial aperture (so different shim d), 3) in terms of qualitative agreement with the measured values and 4) no 'ad-hoc' assumption is needed to determine the coupling stiffness.

Unlike the mentioned qualitative predictive qualities of both the model outcome as the parameter extraction the overall quantitative prediction is inaccurate as e.g. indicated by the mean error which yields 30% in both oscillation regions. Even if this error range is large, it is smaller than obtained in previous studies for which the coupling stiffness is determined in an 'ad-hoc' way [21].

The need for different sets of model parameters to predict both oscillation regions suggest that several mechanical modes are involved. The applied two-mass model can

not account for more than two replica resonances at a same time and is incapable of accounting for modes related to three dimensional movement. Consequently, a more complex mechanical model is of interest to avoid a change of parameters or to account for three dimensional modes.

Conclusion

The presented experimental and modeling study deals with the influence of initial geometrical, acoustical and mechanical conditions on the onset pressure threshold of vocal folds self-sustained oscillation. The following conclusions are made:

- Experimental observations of the onset pressure thresholds and associated oscillation frequencies illustrate the influence of the variation of initial conditions on the self-sustained oscillation behaviour. Variation of initial aperture and mechanical properties results in two oscillation regions for which the difference in onset pressure and resonance frequency yields 1000 Pa and 100 Hz, respectively. In addition the importance of acoustical coupling is apparent for the longest assessed pipe length of 49.5 cm for which the second oscillation regime is absent and the observed oscillation frequency matches the pipes resonance frequency.
- Estimation of the coupling parameter required in the two mass model from the measured frequency response instead of imposing a fixed 'ad-hoc' value yields a qualitative good agreement between predicted and measured oscillation onset pressures for the whole range of assessed initial apertures and mechanical conditions. The relevance of varying the coupling parameter is shown since different values are used for estimation of the onset pressure for different initial geometrical and mechanical conditions. In addition, the same approach is suitable to experimentally estimate the value of the time-delay required in the delayed one-mass model. Consequently, for the mechanical model portion only the critical collision threshold is an 'ad-hoc' parameter. Therefore, future modelling efforts involve improvement of the discrete collision model in order to avoid 'ad-hoc' parameter tuning in case not only the oscillation onset is of interest.
- The used experimental replica is suitable to impose different initial apertures while maintaining mechanical properties as in an abduction or adduction gesture in human phonation. In addition, the mechanical properties of the replica are comparable to human vocal folds with respect to 1) the presence of 2 or 3 mechanical resonance frequencies and 2) the Young's modulus of the replica varies in the same range as measured 'in-vivo'. Furthermore, for a typical vocal tract length of 18 cm acoustical coupling is weak and its influence can be neglected. The outlined experimental estimation of the mechanical coupling parameter is interesting for 'in-vivo' validation of the model with model parameters determined from 'in-vivo' observations of the prephonatory glottal aperture and mechanical properties.

Appendix

A1. Theoretical model and stability analysis

The theoretical symmetrical two-mass model is schematically depicted in Figure A1. In the following the model detailed in [3, 21] is briefly outlined and the parameter γ is introduced. Next, the system equations resulting from a linear stability analysis are derived.

A1.1. Flow model

The flow through the glottal constriction is described assuming a quasi-steady inviscid and incompressible flow corrected for some viscous effects in case of small glottal apertures and flow separation in the diverging portion of the glottis as $A_s(t) = 1.2 \times \min(A(x,t))$. The pressure distribution $P(x,t)$ and volume flow rate Φ is written as:

$$P(x,t) = P_u - \frac{1}{2}\rho\Phi^2\left(\frac{1}{A^2(x,t)} - \frac{1}{A^2(x_0)}\right) + 12\mu w^2\Phi\int_{x_0}^{x}\frac{\mathrm{d}x}{A^3(x,t)}, \quad \text{if } x < x_s, \tag{A1}$$

$$P(x,t) = P_d, \quad \text{if } x \geq x_s, \tag{A2}$$

with w the uniform width of the glottal replica, μ the dynamic viscosity of air and ρ the density of air, so that

$$\Phi = \left[12\mu w^2\Phi\int_{x_0}^{x}\frac{\mathrm{d}x}{A^3(x,t)} + \left\{\left(12\mu w^2\Phi\int_{x_0}^{x}\frac{dx}{A^3(x,t)}\right)^2 + 2(P_u - P_d)\rho\left(1/A_s^2 - 1/A^2(x_0)\right)\right\}^{1/2}\right]\left[\rho\left(1/A_s^2 - 1/A^2(x_0)\right)\right]^{-1}. \tag{A3}$$

A1.2. Mechanical model

Using the notations introduced in section 1, the mechanical model is written as two coupled equations:

$$\frac{m}{2}\frac{\mathrm{d}^2A_1}{\mathrm{d}t^2} + \frac{R}{2}\frac{\mathrm{d}A_1}{\mathrm{d}t} + \frac{K(1+\gamma)}{2}A_1 - \frac{\gamma K}{2}A_2 = F_1(A_1, A_2, P_u, P_d), \tag{A4}$$

$$\frac{m}{2}\frac{\mathrm{d}^2A_2}{\mathrm{d}t^2} + \frac{R}{2}\frac{\mathrm{d}A_2}{\mathrm{d}t} + \frac{K(1+\gamma)}{2}A_2 - \frac{\gamma K}{2}A_1 = F_2(A_1, A_2, P_u, P_d), \tag{A5}$$

with $F_{1,2}$ the force exerted by the fluid on the first and second mass respectively. The mechanical equations at equilibrium reduces to:

$$\frac{K(1+\gamma)}{2}\bar{A}_1 - \frac{\gamma K}{2}\bar{A}_2 = F_1(\bar{A}_1, \bar{A}_2, \bar{P}_u, \bar{P}_d = 0), \tag{A6}$$

$$\frac{K(1+\gamma)}{2}\bar{A}_2 - \frac{\gamma K}{2}\bar{A}_1 = F_2(\bar{A}_1, \bar{A}_2, \bar{P}_u, \bar{P}_d = 0), \tag{A7}$$

from which the equilibrium positions for a given upstream pressure $\bar{P}_u$ are derived by a fixed point method.

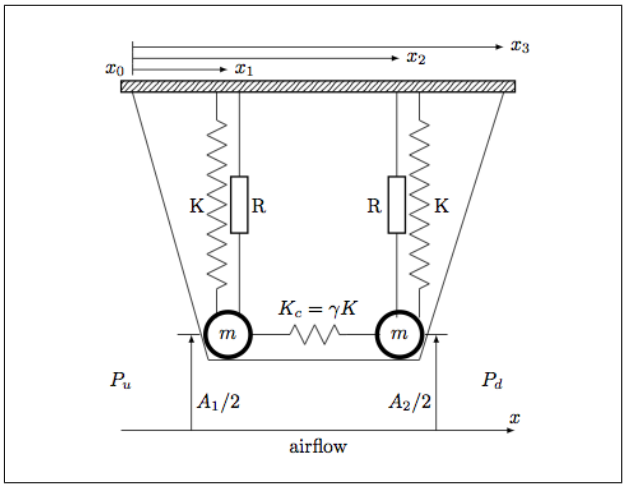

Figure A1. Schematic representation of a symmetrical two mass model [3, 21] introducing the parameter γ.

Assuming a small perturbation (a_1, a_2, p_u, p_d) of the quantities around the equilibrium values $eq = (\bar{A}_1, \bar{A}_2, \bar{P}_u, \bar{P}_d = 0)$ as:

$$A_1 = \bar{A}_1 + a_1, \qquad A_2 = \bar{A}_2 + a_2, \tag{A8}$$

$$P_u = \bar{P}_u + p_u, \qquad P_d = \bar{P}_d + p_d, \tag{A9}$$

results in the following set of equations:

$$\frac{m}{2}\frac{\mathrm{d}^2 a_1}{\mathrm{d}t^2} + \frac{R}{2}\frac{\mathrm{d}a_1}{\mathrm{d}t} + \frac{K(1+\gamma)}{2}a_1 - \frac{\gamma K}{2}a_2 = \frac{\partial F_1}{\partial A_1}\bigg|_{eq} a_1 + \frac{\partial F_1}{\partial A_2}\bigg|_{eq} a_2 + \frac{\partial F_1}{\partial P_u}\bigg|_{eq} p_u + \frac{\partial F_1}{\partial P_d}\bigg|_{eq} p_d, \tag{A10}$$

$$\frac{m}{2}\frac{\mathrm{d}^2 a_2}{\mathrm{d}t^2} + \frac{R}{2}\frac{\mathrm{d}a_2}{\mathrm{d}t} + \frac{K(1+\gamma)}{2}a_2 - \frac{\gamma K}{2}a_1 = \frac{\partial F_2}{\partial A_1}\bigg|_{eq} a_1 + \frac{\partial F_2}{\partial A_2}\bigg|_{eq} a_2 + \frac{\partial F_2}{\partial P_u}\bigg|_{eq} p_u + \frac{\partial F_2}{\partial P_d}\bigg|_{eq} p_d. \tag{A11}$$

A1.3. Acoustic model

The acoustic set of equations is given as

$$\frac{d^2\psi_d}{d^2t} + \frac{\omega_d}{Q_d}\frac{d\psi_d}{dt} + \omega_d^2\psi_d = \frac{Z_d\omega_d}{Q_d}\phi, \tag{A12}$$

$$\frac{d^2\psi_u}{d^2t} + \frac{\omega_u}{Q_d}\frac{d\psi_u}{dt} + \omega_u^2\psi_u = -\frac{Z_u\omega_u}{Q_u}\phi, \tag{A13}$$

with $\partial\psi_{u,d}/\partial t = p_{u,d}$ the acoustic pressure and ϕ the unsteady portion of the volume flow velocity downstream the vocal folds, $\omega_{u,d}$ the acoustical resonance pulsation, $Q_{u,d}$ the quality factor and $Z_{u,d}$ the peak value of the acoustical impedance. As for the mechanical equations assuming small variations around equilibrium results in

$$\frac{\mathrm{d}2\psi_d}{\mathrm{d}^2t} + \frac{\omega_d}{Q_d}\frac{\mathrm{d}\psi_d}{\mathrm{d}t} + \omega_d^2\psi_d = \frac{Z_d\omega_d}{Q_d}\left(\frac{\partial\Phi}{\partial A_1}\bigg|_{eq} a_1 + \frac{\partial\Phi}{\partial A_2}\bigg|_{eq} a_2 + \frac{\partial\Phi}{\partial P_u}\bigg|_{eq} p_u + \frac{\partial\Phi}{\partial P_d}\bigg|_{eq} p_d\right), \tag{A14}$$

$$\frac{\mathrm{d}^2\psi_u}{\mathrm{d}^2t} + \frac{\omega_u}{Q_d}\frac{\mathrm{d}\psi_u}{\mathrm{d}t} + \omega_u^2\psi_u = -\frac{Z_u\omega_u}{Q_u}\left(\frac{\partial\Phi}{\partial A_1}\bigg|_{eq} a_1 + \frac{\partial\Phi}{\partial A_2}\bigg|_{eq} a_2 + \frac{\partial\Phi}{\partial P_u}\bigg|_{eq} p_u + \frac{\partial\Phi}{\partial P_d}\bigg|_{eq} p_d\right). \tag{A15}$$

A1.4. Linear stability analysis

Consequently, assuming small variations around equilibrium results in a coupled set of equations obtained from (A10), (A11), (A14) and (A15):

$$m\frac{\mathrm{d}^2 a_1}{\mathrm{d}t^2} + R\frac{\mathrm{d}a_1}{\mathrm{d}t} - 2\frac{\partial F_1}{\partial P_u}\bigg|_{eq}\frac{\mathrm{d}\psi_u}{\mathrm{d}t} - 2\frac{\partial F_1}{\partial P_d}\bigg|_{eq}\frac{\mathrm{d}\psi_d}{\mathrm{d}t} + \left(K(1+\gamma) - 2\frac{\partial F_1}{\partial A_1}\bigg|_{eq}\right)a_1 - \left(\gamma K + 2\frac{\partial F_1}{\partial A_2}\bigg|_{eq}\right)a_2 = 0, \tag{A16}$$

$$m\frac{\mathrm{d}^2 a_2}{\mathrm{d}t^2} + R\frac{\mathrm{d}a_2}{\mathrm{d}t} - 2\frac{\partial F_2}{\partial P_u}\bigg|_{eq}\frac{\mathrm{d}\psi_u}{\mathrm{d}t} - 2\frac{\partial F_2}{\partial P_d}\bigg|_{eq}\frac{\mathrm{d}\psi_d}{\mathrm{d}t} - \left(\gamma K + 2\frac{\partial F_2}{\partial A_1}\bigg|_{eq}\right)a_1 + \left(K(1+\gamma) - 2\frac{\partial F_2}{\partial A_2}\bigg|_{eq}\right)a_2 = 0, \tag{A17}$$

$$\frac{\mathrm{d}^2\psi_d}{\mathrm{d}^2t} - \frac{Z_d\omega_d}{Q_d}\frac{\partial\Phi}{\partial P_u}\bigg|_{eq}\frac{\mathrm{d}\psi_u}{\mathrm{d}t} + \left(\frac{\omega_d}{Q_d} - \frac{Z_d\omega_d}{Q_d}\frac{\partial\Phi}{\partial P_d}\bigg|_{eq}\right)\frac{\mathrm{d}\psi_d}{\mathrm{d}t} - \frac{Z_d\omega_d}{Q_d}\frac{\partial\Phi}{\partial A_1}\bigg|_{eq}a_1 - \frac{Z_d\omega_d}{Q_d}\frac{\partial\Phi}{\partial A_2}\bigg|_{eq}a_2 + \omega_d^2\psi_d = 0, \tag{A18}$$

$$\frac{\mathrm{d}^2\psi_u}{\mathrm{d}^2t} + \left(\frac{\omega_u}{Q_d} + \frac{Z_u\omega_u}{Q_u}\frac{\partial\Phi}{\partial P_u}\bigg|_{eq}\right)\frac{\mathrm{d}\psi_u}{\mathrm{d}t} + \frac{Z_u\omega_u}{Q_u}\frac{\partial\Phi}{\partial P_d}\bigg|_{eq}\frac{\mathrm{d}\psi_d}{\mathrm{d}t} + \frac{Z_u\omega_u}{Q_u}\frac{\partial\Phi}{\partial A_1}\bigg|_{eq}a_1 + \frac{Z_u\omega_u}{Q_u}\frac{\partial\Phi}{\partial A_2}\bigg|_{eq}a_2 + \omega_u^2\psi_u = 0. \tag{A19}$$

The system can be expressed in state-space form as

$$\dot{X} = MX \tag{A20}$$

with $X = [a_1, a_2, \psi_u, \psi_d, \mathrm{d}a_1/\mathrm{d}t, \mathrm{d}a_2/\mathrm{d}t, \mathrm{d}\psi_u/\mathrm{d}t, \mathrm{d}\psi_d/\mathrm{d}t]$ and M defined as

$$M = \left[\begin{array}{cccc|cccc} 0 & 0 & 0 & 0 & 1 & 0 & 0 & 0 \\ 0 & 0 & 0 & 0 & 0 & 1 & 0 & 0 \\ 0 & 0 & 0 & 0 & 0 & 0 & 1 & 0 \\ 0 & 0 & 0 & 0 & 0 & 0 & 0 & 1 \\ \hline -\frac{K(1+\gamma)-2\frac{\partial F_1}{dA_1}|_{eq}}{m} & \frac{\gamma K+2\frac{\partial F_1}{dA_2}|_{eq}}{m} & 0 & 0 & -\frac{R}{m} & 0 & \frac{2}{m}\frac{\partial F_1}{\partial P_u}\Big|_{eq} & \frac{2}{m}\frac{\partial F_1}{\partial P_d}\Big|_{eq} \\ \frac{\gamma K+2\frac{\partial F_2}{dA_1}|_{eq}}{m} & -\frac{K(1+\gamma)-2\frac{\partial F_2}{dA_2}|_{eq}}{m} & 0 & 0 & 0 & -\frac{R}{m} & \frac{2}{m}\frac{\partial F_2}{\partial P_u}\Big|_{eq} & \frac{2}{m}\frac{\partial F_2}{\partial P_d}\Big|_{eq} \\ \frac{Z_d\omega_d}{Q_d}\frac{\partial\Phi}{\partial A_1}\Big|_{eq} & \frac{Z_d\omega_d}{Q_d}\frac{\partial\Phi}{\partial A_2}\Big|_{eq} & 0 & -\omega_d^2 & 0 & 0 & \frac{Z_d\omega_d}{Q_d}\frac{\partial\Phi}{\partial P_u}\Big|_{eq} & -\left(\frac{\omega_d}{Q_d} - \frac{Z_d\omega_d}{Q_d}\frac{\partial\Phi}{\partial P_d}\Big|_{eq}\right) \\ -\frac{Z_u\omega_u}{Q_u}\frac{\partial\Phi}{\partial A_1}\Big|_{eq} & -\frac{Z_u\omega_u}{Q_u}\frac{\partial\Phi}{\partial A_2}\Big|_{eq} & -\omega_u^2 & 0 & 0 & 0 & -\left(\frac{\omega_u}{Q_d} + \frac{Z_u\omega_u}{Q_u}\frac{\partial\Phi}{\partial P_u}\Big|_{eq}\right) & -\frac{Z_u\omega_u}{Q_u}\frac{\partial\Phi}{\partial P_d}\Big|_{eq} \end{array}\right]$$

For a known set of initial conditions the system will become instable, corresponding to oscillation onset, in case the real portion of an eigenvalue of M is positive. The corresponding oscillation pulsation is obtained as the imaginary portion of the eigenvalue.

Note that in the foregoing collision is detected following the criterion $h_c = A/w < h_{crit}$ in which case the values of K and R are increased to $K = 4K$ and $R = R + 2\sqrt{Km}$. The fixed collision threshold h_{crit} is set to 0.02 mm.

References

[1] J. L. Flanagan, L. L. Landgraf: Self oscillating source for vocal tract synthesizers. IEEE Trans. on Audio and Electroacoustics **16** (1968) 57–64.

[2] K. Ishizaka, J. Flanagan: Synthesis of voiced sounds from a two-mass model of the vocal cords. Bell Syst. Tech. J. **51** (1972) 1233–1267.

[3] N. J. C. Lous, G. C. J. Hofmans, R. N. J. Veldhuis, A. Hirschberg: A symmetrical two-mass vocal-fold model coupled to vocal tract and trachea, with application to prosthesis design. Acta Acustica **84** (1998) 1135–1150.

[4] J. G. Svec, J. Horacek, F. Sram, J. Vesely: Resonance properties of the vocal folds: in vivo laryngoscopic investigation of the externally excited laryngeal vibrations. J. Acoust. Soc. Am. **108** (2000) 1397–1406.

[5] M. Newton, D. M. Campbell, J. Gilbert: Mechanical response measurements of real and artificial brass players lips. J. Acoust. Soc. Am. **123** (2008) 7.

[6] K. Tsunoda, Y. Ohta, Y. Soda, S. Niimi, H. Hirose: Laryngeal adjustment in whispering magnetic resonance imaging study. Ann Otol Rhinol Laryngol **106** (1997) 41–43.

[7] J. Poletto, L. Verdun, R. Strominger, L. Ludlow: Correspondence between laryngeal vocal fold movement and muscle activity during speech and nonspeech gestures. J Appl Physiol. **97** (2004) 858–866.

[8] E. J. Hunter, I. R. Titze, F. Alipour: A three-dimensional model of vocal fold abduction/adduction. J. Acoust. Soc. Am. **115** (2004) 1747–1759.

[9] A. D. Rubin, V. Praneetvatakul, S. Gherson, C. A. Moyer, R. T. Sataloff: Laryngeal hyperfunction during whispering: Reality or myth? Journal of Voice **20** (2006) 121–127.

[10] Q. T. Tran, S. G. Berke, B. R. Gerratt, J. Kreiman: Measurement of Young's modulus in the in vivo human vocal folds. Annals of otology, rhinology and laryngology **102** (1993) 584–591.

[11] Y. B. Min, I. R. Titze, F. Alipour: Stress-strain response of the human vocal ligament. Ann. Otol. Rhinol. Laryngol. **104** (1995) 563–569.

[12] J. Van den Berg, J. T. Zantema, P. Doornenbal: On the air resistance and the Bernoulli effect of the human larynx. J. Acoust. Soc. Am. **29** (1957) 626–631.

[13] A. Barney, C. H. Shadle, P. O. A. L. Davies: Fluid flow in a dynamic mechanical model of the vocal folds and tract. i. measurements and theory. J. Acoust. Soc. Am. **105** (1999) 444–455.

[14] I. R. Titze, S. S. Schmidt, M. R. Titze: Phonation threshold pressure in a physical model of the vocal fold mucosa. J. Acoust. Soc. Am. **97** (1995) 3080–3084.

[15] D. Shinwari, R. C. Scherer, K. J. DeWitt, A. A. Afjeh: Flow visualization and pressure distributions in a model of the glottis with a symmetric and oblique divergent angle of 10 degrees. J. Acoust. Soc. Am. **113** (2003) 487–497.

[16] S. Thomson, L. Mongeau, S. Frankel, J. Neubauer, D. Berry: Self-oscillating laryngeal models for vocal fold research. Proc. Flow induced vibrations, Paris, France, 2004, 137–142.

[17] C. Vilain, X. Pelorson, C. Fraysse, M. Deverge, A. Hirschberg, J. Willems: Experimental validation of a quasi-steady theory for the flow through the glottis. J. of Sound and Vibration **276** (2004) 475–490.

[18] M. Triep, C. Brucker, W. Schroder: High-speed PIV measurements of the flow downstream of a dynamic mechanical model of the human vocal folds. Experiments in Fluids **39** (2005) 232–245.

[19] I. Titze: Nonlinear source-filter coupling in phonation: Theory. J. Acoust. Soc. Am. **123** (2008) 2733–2749.

[20] M. Howe, R. McGowan: Analysis of flow-structure coupling in a mechanical model of the vocal folds and the subglottal system. J. Fluids and Structures **25** (2009) 1299–1317.

[21] N. Ruty, X. Pelorson, A. Van Hirtum, I. Lopez, A. Hirschberg: An in-vitro setup to test the relevance and the accuracy of low-order vocal folds models. J. Acoust. Soc. Am. **121** (2007) 479–490.

[22] X. Pelorson, A. Hirschberg, R. R. Van Hasselt, A. P. J. Wijnands, Y. Auregan: Theoretical and experimental study of quasisteady-flow separation within the glottis during phonation. application to a modified two-mass model. J. Acoust. Soc. Am. **96** (1994) 3416–3431.

[23] A. Van Hirtum, J. Cisonni, N. Ruty, X. Pelorson, I. Lopez, F. van Uittert: Experimental validation of some issues in lip and vocal fold physical models. Acta Acustica **93** (2007) 314–323.

[24] Z. Zhang, J. Neubauer, D. Berry: The influence of subglottal acoustics on laboratory models of phonation. J. Acoust. Soc. Am. **120** (2006) 1558–1569.

[25] J. S. Cullen, J. Gilbert, D. M. Campbell: Brass instruments: linear stability analysis and experiments with an artificial mouth. Acta Acustica **86** (2000) 704–724.

[26] S. Sastry: Nonlinear systems : analysis, stability and control. Springer-Verlag, New York, 1999.